Volume 1 | Number 1 | Jan 2013 | Pages 1–100

# Nanoscale

www.rsc.org/nanoscale

ROYAL SOCIETY OF CHEMISTRY

ROYAL SOCIETY OF CHEMISTRY

www.rsc.org/nanoscale

# Journal Name

ROYAL SOCIETY OF CHEMISTRY

## ARTICLE TYPE

# Highly conformal fabrication of nanopatterns on non-planar surfaces

Inès Massiot,[a‡] Christos Trompoukis,[b‡] Kristof Lodewijks,[a] Valérie Depauw,[b] and Alexandre Dmitriev [*a]

While the number of techniques for patterning materials at the nanoscale exponentially increases, only a handful of methods approach the conformal patterning of strongly non-planar surfaces. Here, using the direct surface self-assembly of colloids by electrostatics, we produce highly conformal bottom-up nanopatterns with a short-range order. We illustrate the potential of this approach by devising functional nanopatterns on highly non-planar substrates such as pyramid-textured silicon substrates and inherently rough polycrystalline films. We further produce functionalized polycrystalline thin-film silicon solar cells with enhanced optical performance. The perspective presented here to pattern essentially any surface at the nanoscale, in particular surfaces with high inherent roughness or with microscale features, opens new possibilities in a wide range of advanced technologies from affordable photovoltaics and optoelectronics to cellular engineering.

## 1 Introduction

Numerous top-down and bottom-up nanopatterning techniques are increasingly available with the rapid progress in materials engineering. However, patterning non-planar surfaces of various materials still remains an overwhelming challenge. The ability to pattern any given surface on the nanoscale, in particular surfaces with high inherent roughness or with pre-patterned microscale features, opens new perspectives in various fields from multi-scale biomimetics to optoelectronics. To address this challenge, top-down methods such as soft lithography [1,2] rely on the use of a soft elastomer as a patterning stamp or, like with electron-beam lithography, [3] on the continuous adjustment of the plane of the electron beam focus to take into account the height variations on the substrate. An appealing alternative is the bottom-up self-assembly such as colloidal lithography that offers affordability, high throughput and the possibility of parallel macroscopic area processing. [4–8] The air-water interface colloidal self-assembly is used to form monolayer colloidal crystals on flat and curved surfaces such as glass or ceramic tubes and carbon fibers, leading to close-packed [4–6] or sparse [7] particles arrangements. However, these attempts are limited to surfaces without sharp features as it is not possible to retain the periodic order of the pattern, for example, on pyramid-textured substrates. [8]

We present a bottom-up nanopatterning by the direct surface self-assembly of colloids via electrostatic forces, leading to a highly conformal substrate modification with a short-range ordered pattern of nanofeatures. The resulting nanopattern is an arrangement of nanoscale features, distinct in size and distribution, that could bestow a new function to the surface of the patterned material such as, for example, enhanced interaction with light, [9–12] precisely engineered catalytic activity [13] or designed cellular mechanotransduction [14] and biomimetic adhesion. [9,15,16] Envisioned perspectives include the fabrication of functional nanocavities on non-planar substrates serving as preferential sites for cellular growth [17] or templates for catalyst-free selective epitaxial growth of semiconductor nanowires. [18] Furthermore, the development of the field of disordered photonics has highlighted the remarkable light-matter coupling in amorphous photonic structures due to the short-range order. [19] Efficient broadband absorption has been evidenced in disordered semiconductor films with lower angular dispersion than their periodic counterparts thus offering a new strategy towards high-efficiency thin-film solar cells [20–24] or for light sources applica-

[a] Department of Applied Physics, Chalmers University of Technology, SE-41296, Göteborg, Sweden. E-mail: alexd@chalmers.se.
[b] IMEC, Kapeldreef 75, B-3001 Leuven, Belgium.
‡ These authors contributed equally to this work.

tions, from light-emitting diodes[25] to lasers.[26] The conformal amorphous nanopatterns thus enable light management devices produced with a time-efficient, low-cost and high-throughput bottom-up process. Here we illustrate the broad potential of our approach by devising conformal nanopatterns on highly non-planar substrates such as inherently rough polycrystalline silicon films and pyramid-textured silicon wafers. In both cases, we show that the proposed bottom-up process enables a conformal structuring of the entire surface while retaining the amorphous pattern despite the topography of the substrate.

## 2 Results and discussion

Figure 1 illustrates the process for the conformal bottom-up nanopatterning of non-planar surfaces. First, negatively surface-charged polystyrene (PS) beads are self-assembled by electrostatics onto a non-planar silicon substrate (Fig. 1a) pre-coated with a positively charged triple-layer polymer film. The arrangement of the beads results from the equilibrium between two coexisting electrostatic interactions, the particle-particle repulsion and particle-substrate attraction. The colloidal self-assembly effectively leads to a conformal adsorption of the beads with a very high tolerance to the surface roughness (Fig. 1b). A metal mask (50 nm-thick aluminum film in this case) is then evaporated on the PS spheres to create the etch mask upon spheres removal (Fig 1c). Finally, the samples are etched (here with isotropic reactive ion etching (RIE) with a mixture of $O_2$ and $SF_6$ gases), leading to a substrate with a conformal short-range ordered pattern of nanoholes (Fig. 1d). More details on the process are given in the Experimental section. Although here we focus on silicon surfaces as described in more details in the following, this technique can be widely tuned for different applications with various substrates. The use of a charged polymer thin film allows screening the effect of the surface charges of the native substrate. As a consequence, such bottom-up patterning can be applied to virtually any surface regardless of its material, charge and roughness. Furthermore, this method can be used to produce nanodisks or nanoholes of various shapes. For example, nanodisk features could be derived from the process described in Fig. 1 by depositing a continuous (metal) film prior to colloidal self-assembly. The beads are then used as a selective etch mask of the metal film, thereby leaving, after beads removal, only nanodisk features that in turn can be used as a substrate etch mask and later removed. Finally, the parameters of the short-range ordered pattern (features size and inter-features distance) can be tuned through the parameters of the colloidal self-assembly (size of PS spheres, ionic strength of the solution) and of the etching process. In the case of nanoholes, the profile can be designed depending on the type of the substrate etch (isotropic or anisotropic). Using this method, conformal nanopatterning was achieved on large-area samples (up to 25 $cm^2$, see Figs. 4a and 5a) with very few defects. The processed
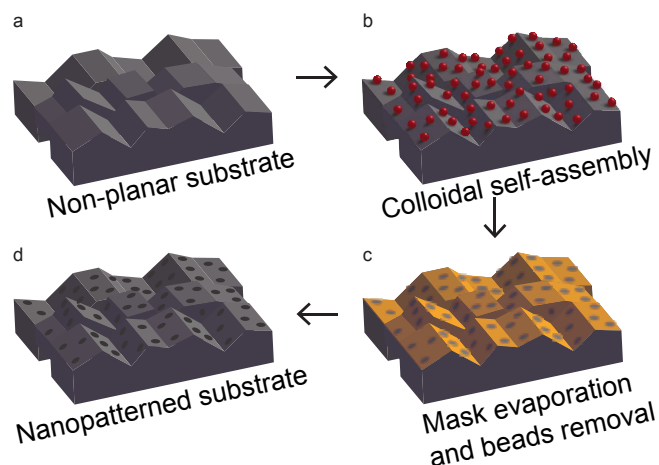


**Fig. 1** Conformal bottom-up nanopatterning of non-planar substrates. (a,b) Adsorption of colloids from aqueous solution onto a rough or micro-structured substrate of choice. (c) Etch mask deposition and beads removal. (d) Etch of the target substrate and removal of the mask.

surface area is only limited in practice by the substrate handling. It is noteworthy that in the case of planar substrates, we have demonstrated that this patterning method could be upscaled to substrates as large as 100 $cm^2$.

Figure 2 illustrates the application of the conformal patterning method to non-planar substrates with a high native roughness. We have used 3 $\mu$m-thick polycrystalline silicon thin films grown on alumina substrates by aluminium-induced crystallization. This material is inherently rough and, as micrometer thin crystalline silicon films, suffers from incomplete light absorption due to its thickness. It thus requires advanced light management schemes to enable efficient light absorption and therefore be integrated in efficient solar cells.[27] PolySi substrates, as polycrystalline materials in general, exhibit a native roughness that can be up to the micron scale (Fig. 2a), which represents a real challenge for the surface functionalization of the material. Nevertheless, as shown on SEM images (Figs. 2b-c), the metal mask obtained after colloidal self-assembly and metal evaporation exhibits a perfect conformity to such rough surface, very efficiently adapting to the highly varied relief, from the wrinkled valleys (Fig. 2b) to the steep slopes (Fig. 2c). The short-range order of nanoholes arrangement in the mask persists on the steep slopes, with a slight distortion of the nanohole lateral size as the slope angle increases due to the directional metal evaporation.

As mentioned previously, the geometric characteristics of the hole pattern, namely the size of the holes and the pattern filling fraction - ratio between the area covered by the holes and the total area - depend on the initial bead size. Fig. 2d displays SEM images of patterns obtained with initial bead sizes of 270 (final hole diameter = 550 nm), 410 (final hole diameter = 600 nm) and 510 nm (final hole diameter = 800 nm) to illustrate the im-
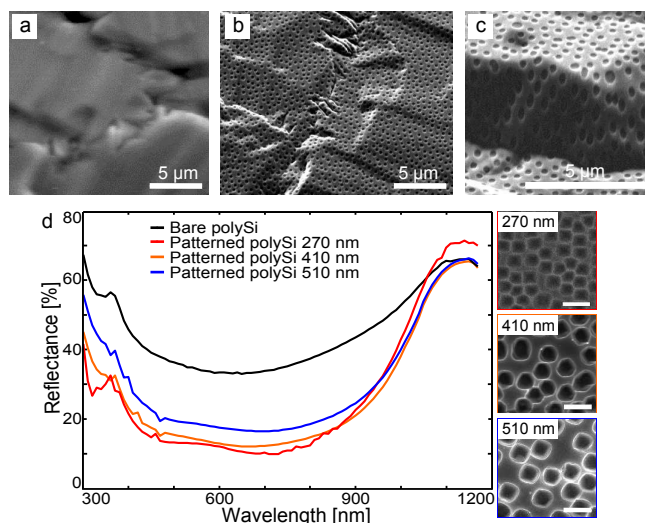
**Fig. 2** Conformal bottom-up nanopatterning of inherently rough polycrystalline thin-film silicon (polySi) substrates. (a) SEM image of a native polySi substrate. (b,c) SEM images of a polySi surface with a metal etch mask (nominal bead size = 270 nm) showing its conformity to the rough surface. (d) Reflectance of nanopatterned polySi with nominal bead sizes from 270 to 510 nm, compared to the native polySi surface (black). Top-view SEM images of the corresponding nanopatterned surfaces are shown to the right with a scale bar of 1 micron.

pact of the bead size on the pattern, all the other parameters of the colloidal self-assembly and etch steps being the same. The filling fraction of the beads pattern standardly obtained after colloidal self-assembly is 10 to 20 %. Lower filling fractions can be reached either by using lower concentration of the colloidal solution, or larger beads and a plasma treatment to shrink the beads to the desired hole size.[28] Higher filling fractions of the pattern are achieved by increasing the ionic strength of the colloidal solution in order to screen the colloids surface charge and decrease the interparticle repulsion.[28] Additionally, the final filling fraction of the pattern can be changed by tuning the parameters of the etch process. As reported in a previous publication,[29] we have demonstrated that a filling fraction higher than 90 % could be achieved by optimizing the dry etch time.

We probe the functionality of the produced pattern by comparing the optical reflection of the patterned substrates with a native polySi surface. As displayed in Fig. 2d, for all nanohole sizes, the conformal nanopattern induces a significant decrease in the reflectance of the native polySi surface in the entire visible range. In particular, for the nominal bead size of 270 nm, we demonstrate a drop in the integrated reflectance from 41.7 % to 22.6 %. This drop in reflectance can be attributed to a better light in-coupling (short wavelengths) and light-trapping (long wavelengths) in the nanopatterned sample. At short wavelengths, the conformal nanopattern effectively provides a gradient in the

refractive index from air to bulk silicon leading to a strong antireflection effect. This effect becomes less efficient as the filling fraction decreases (i.e. for larger beads), in agreement with a recently published work,[30] hence the lowest reflectance is achieved for a bead size of 270 nm. At longer wavelengths, the nanopattern enables the excitation of guided modes in the polySi film thereby inducing an efficient light-trapping of photons that were not trapped in a single pass. The amorphous nature of the pattern leads to a higher number of guided modes than in the case of a periodic pattern, which also means that the absorption will be less dependent on the angle of incidence of the impinging photons[22].

The patterning of polySi substrates using the proposed process reveals two major advantages over previously developed strategies. Firstly, as shown in Fig. 2b, due to the strong attractive electrostatic interactions between the particles and the substrate, the short-range order in the functional pattern is retained regardless of the relief of the substrate. Second, the bottom-up conformal nanopatterning compares favorably to the top-down nanoimprint lithography (NIL) technique standardly used for periodic patterning, as illustrated in Fig. 3. The high tolerance of the bottom-up patterning technique to the topography of the substrate enables to pattern the entire surface (Fig. 3a).

In the next step we test the suitability of the conformal bottom-up nanopatterning for optoelectronic devices on polycrystalline silicon solar cells. Polycrystalline silicon is a thin-film photovoltaics material that is grown directly from vapor or liquid phase on foreign substrates, thus offering a low-cost alternative to monocrystalline silicon solar cells.[31,32] Furthermore, achieving broadband efficient light absorption in thin semiconductor films is a crucial task for the future of solar energy use, as one of the routes to cost reduction is to design highly efficient ultrathin devices. We foresee that the light-management bottom-up nanopatterns developed here are relevant to a wide range of photovoltaic materials, from ultrathin monocrystalline silicon films to rough polycrystalline materials such as $CuInGaSe_2$. The bottom-up conformal nanopatterns thus propose a generic strategy to
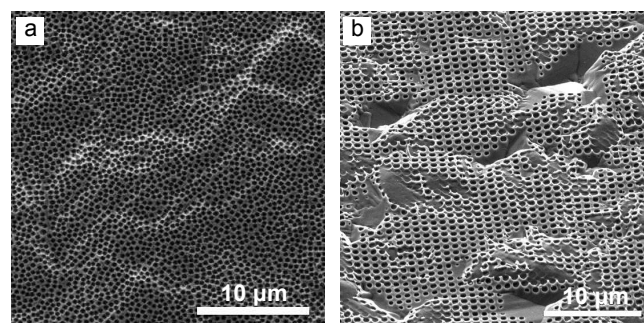


**Fig. 3** Comparison of polySi surface patterned by bottom-up nanopatterning (a) and nanoimprint lithography (b).
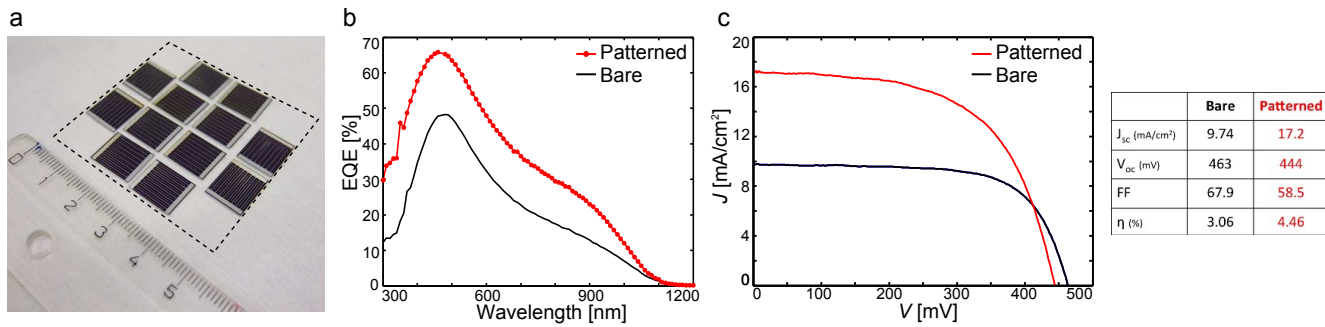
**Fig. 4** PolySi solar cells enhanced by conformal bottom-up nanopatterning (nominal bead size of 270 nm). (a) Photograph of the nanopatterned polySi cells (1 x 1 cm). The initial size of the nanopatterned polySi wafer before dicing (5 x 5 cm) is shown with dashed lines. (b,c) Electrical performances of a native polySi cell (black) and the best obtained nanopatterned polySi cell (red).

wards nanophotonic light-trapping solutions for high-efficiency thin-film solar cells, with spectral and angular properties tunable with the nanohole size and the short-range order of the holes arrangement. Here nanopattern-enhanced polySi surfaces, as the ones described previously, are integrated into a photovoltaic device using an heterojunction structure with interdigitated contacts (Fig. 4, for cell fabrication details see Experimental section). Fig. 4a shows a photograph of nanopatterned polySi cells (1 x 1 cm) made by dicing the original nanopatterned polySi substrate (5 x 5 cm, dashed lines). Fig. 4b displays the external quantum efficiency (EQE) measurements, i.e. the ratio of the number of carriers collected in the solar cell to the number of incident photons as a function of the incident wavelength, on the best obtained cell. As a consequence of the strongly reduced reflectance discussed previously, the nanopatterned cell (red) exhibits a substantial increase in the EQE compared to the reference cell (black), thereby leading to an increase in the short-circuit current density from 9.74 for the reference cell to 17.2 mA/cm$^2$ for the patterned cell. The impressive gain in the optical performance of the cell is compromised to some extent in the present case by the open-circuit voltage and fill factor losses (Fig. 4c). The reduced electrical performances (see table in Fig. 4c) can be attributed to the material damage due to dry etch and the non-conformal contacts deposition, leading to significant recombination and collection losses on the front compared to the reference cell.[33] Still, close to 50 % increase in the conversion efficiency is observed from 3.06 % for the reference cell to 4.46 % for the device with the conformal nanopattern. We foresee that advances in electrical passivation of the nanopatterned surfaces along with better contact engineering would prevent the drop in the electrical performance and would lead to further efficiency increase for the polySi cells with conformal nanopatterns. Despite the fact that the bare pc-Si cells in this study do not have the highest efficiency obtained in our labs[27], the relative increase in the short-circuit current density observed in the case of the nanopatterned cells clearly demonstrates the potential of our patterning technique.

To demonstrate the process conformity to sharp features, we proceed with patterning a random pyramid-textured silicon surface as displayed in Fig. 5. Etching (100)-oriented Si by an anisotropic wet etchant (tetramethylammonium hydroxide) results in a random distribution of micron-sized pyramids with steep 54.7° slopes. The pyramid-textured surface is then functionalized with a bottom-up conformal nanopattern employing a 50 nm-thick Al mask with 270 nm-diameter nanoholes and isotropic RIE. As shown in Fig. 5a, the Al etch mask exhibits perfect topography-independent coverage of the surface, retaining the short-range order as on a flat substrate. The use of a pyramid-textured substrate highlights the true three-dimensional conformity of the approach, as the nanohole-patterned mask accommodates all the facets, and even the very tips, of the micro-pyramids of the substrate (Fig. 5b). The dry etch and mask removal reveal an intricate multiscale surface texture formed by the short-range ordered pattern of sub-wavelength parabolic nanoholes, conforming to the micron-sized pyramids (Fig. 5c). Random pyramid texturing of silicon[35] is conventionally implemented in solar cell devices to increase the photon absorption probability compared to a flat surface using the ray optics effect. It generally leads to a drop in the reflectance (integrated from 300 to 1170 nm) from 34 % for a flat silicon wafer substrate to 12 % after random pyramid texturing.[36] Here, the conformal nanopattern effectively provides a graded index effect leading to a further drop in the integrated reflectance from 12 % to 8.9 %. In principle, to push the reflectivity further down, the nanoholes aspect ratio should be increased.[37–39] In the context of light-trapping for solar cells, recent work has proposed a similar approach based on a modulated surface texture combining nanocones and micropyramids in order to achieve broadband absorption.[40] However, in this approach, the geometry of the original microscale features is significantly affected by the nanopatterning process, which can be crucial in applications beyond photovoltaics. In a broader perspective, the very high tolerance of the fabricated nanopatterns to the substrate relief, as illustrated in the case of random pyramid-
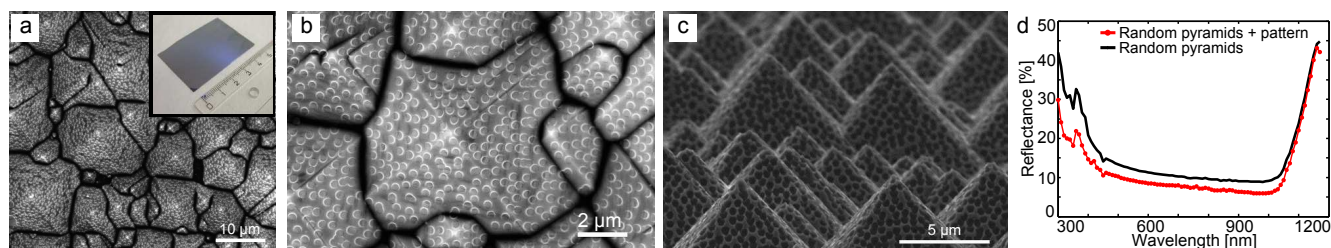
**Fig. 5** Conformal bottom-up nanopatterning of pyramid-textured silicon substrates. (a,b) SEM images of pyramid-textured substrates with a metal etch mask. Inset in a: photograph of the nanopatterned substrate (5 x 5 cm). (c) Side view of a nanopatterned pyramid-textured substrate after dry etch and mask removal. (d) Reflectance of a pristine pyramid-textured surface (black) and a surface with added conformal nanopattern (red, nominal bead size of 270 nm).

textured substrates, prompts the conformal patterning of fully three dimensional, micro- or macroscopic, objects with potentially steep topography. In particular, it opens new possibilities for the realization of biomimetic multifunctional landscapes,[9] where the conformal bottom-up nanopattern would confer an additional functionality to the substrate from surface (adhesion, wetting) to optical properties. We also mention here the increase of the effective surface area as a result of conformal nanopatterning. This might be decisive for the potential heterogeneous nanocatalysis applications of such patterned surfaces.

## 3　Conclusions

In conclusion, we have devised a class of conformal bottom-up nanopatterns that bestow an additional functionality to largely non-planar or 3D-structured surfaces. The nanopatterns are produced on macroscopic areas by affordable colloidal self-assembly-based nanofabrication, suitable to structure a wide range of materials with (nano)features. Here we have focused on the enhanced light-matter interaction in silicon substrates for applications to photovoltaics. We have illustrated the high tolerance of these patterns to surface roughness by fabricating them conformally on 3D micro-pyramids, boosting the antireflective properties of the surface. As a proof-of-concept of applications to optoelectronic devices, we have demonstrated the potential of bottom-up amorphous photonic nanostructures for light management in polycrystalline thin-film silicon photovoltaic devices by showing a significant improvement of the short-circuit current density thanks to patterning. In a broader context, the high conformity of the bottom-up nanopatterns to the various surface reliefs opens new perspectives towards the fabrication of functional multiscale surfaces. This work paves the way towards the nanopatterning of virtually any nano-, micro- or macroscopic three-dimensional objects, including sharp stand-alone features and vertical sidewalls.

## 4　Experimental details

### 4.1　Self-assembly of polystyrene particles

For all the bottom-up nanopatterned samples presented in this paper, a triple-polymer layer was adsorbed onto the substrate prior to self-assembly: (i) PDDA (poly(diallyldimethylammonium chloride), 0.2 wt %, Sigma Aldrich); (ii) PSS (poly(sodium 4-styrenesulfonate), 2 wt %, Sigma Aldrich); (iii) ACH (aluminium chloride hydroxide, 5 wt %, Summit Reheis). In between each adsorption step, the sample was rinsed under deionized (DI) water and dried under nitrogen flow. A solution of negatively-charged polystyrene (PS) particles (sulfate latex, Life technologies, concentration 0.2 wt %) was then dropcast onto the sample and let to adsorb for 2 minutes to reach saturation of the surface. The sample was rinsed under running DI water to wash away the excess particles and dried under nitrogen flow. A heat treatment of the PS particles was performed during rinsing to avoid aggregation of the particles upon drying. After evaporation of an aluminum mask (50 nm thickness), the PS beads were removed by a soft wiping of the surface in acetone.

### 4.2　Dry plasma etching

After beads removal, the samples were etched with reactive ion etching with a mixture of $SF_6$ and $O_2$ gases (100/30 sccm) at 100 mTorr pressure and a power of 100 W, leading to an arrangement of subwavelength parabolic holes of about 600 nm in diameter for a nominal bead size of 270 nm.

### 4.3　Nanoimprint lithography

The samples were pressed under a soft stamp with a hydraulic press at 130°C and 20 bar, after spinning a thermoplastic resist. The resist was mr-I 7010R from Micro-resist technologies and the soft stamp was Sylgard 184, a silicone elastomer from Dow Corning.

## 4.4 Polycrystalline silicon solar cells

Polycrystalline silicon films were grown by aluminium-induced crystallization on alumina substrates, as described in a previous work.[27,33] After nanopatterning with the bottom-up process described previously, an heterojunction structure was made by deposition of an amorphous silicon emitter followed by sputtering of an indium tin oxide window layer. The cells were completed by the deposition of interdigitated front contacts (silver for the emitter and aluminum for the base) through photolithography, electron beam evaporation and lift-off.

## 5 Acknowledgements

## References

1 Y. Xia and G. M. Whitesides, *Annu. Rev. Mater. Sci.*, 1998, **28**, 153–184.

2 J. P. Rolland, E. C. Hagberg, G. M. Denison, K. R. Carter and J. M. De Simone, *Angew. Chemie - Int. Ed.*, 2004, **43**, 5796–5799.

3 V. Ray, Y. Aida, R. Funakoshi, H. Kato and S. W. Pang, *J. Vac. Sci. Technol. B*, 2012, **30**, 06F303.

4 S. A. Pendergraph, J. Y. Park, N. R. Hendricks, A. J. Crosby and K. R. Carter, *Small*, 2013, **9**, 3037–3042.

5 S. Xu, F. Sun, F. Gu, Y. Zuo, L. Zhang, C. Fan, S. Yang and W. Li, *ACS Appl. Mater. Interfaces*, 2014, **6**, 1251–1257.

6 B. L. Jia and W. Cai, *Adv. Funct. Mater.*, 2010, **20**, 3765–3773.

7 S. P. Bhawalkar, J. Qian, M. C. Heiber and L. Jia, *Langmuir*, 2010, **26**, 16662–16666.

8 E. M. Akinoglu, A. J. Morfa and M. Giersig, *Turkish J. Phys.*, 2014, **38**, 563–572.

9 W. G. Bae, H. N. Kim, D. Kim, S. H. Park, H. E. Jeong and K. Y. Suh, *Adv. Mater.*, 2014, **26**, 675–699.

10 A. R. Parker and H. E. Townley, *Nat. Nanotechnol.*, 2007, **2**, 347–353.

11 W. Wang, W. Zhang, X. Fang, Y. Huang, Q. Liu, M. Bai and D. Zhang, *Opt. Lett.*, 2014, **39**, 4208–4211.

12 D. Franklin, Y. Chen, A. Vazquez-Guardado, S. Modak, J. Boroumand, D. Xu, S.-T. Wu and D. Chanda, *Nat. Commun.*, 2015, **6**, 7337.

13 M. Shakeri, L. Roiban, V. Yazerski, G. Prieto, R. J. M. Klein Gebbink, P. E. de Jongh and K. P. D. Jong, *ACS Catal.*, 2014, **4**, 3791–3796.

14 J. E. Gautrot, J. Malmström, M. Sundh, C. Margadant, A. Sonnenberg and D. S. Sutherland, *Nano Lett.*, 2014, **14**, 3945–3952.

15 M. K. Kwak, H. E. Jeong and K. Y. Suh, *Adv. Mater.*, 2011, **23**, 3949–3953.

16 S. Y. Yang, E. D. O'Cearbhaill, G. C. Sisk, K. M. Park, W. K. Cho, M. Villiger, B. E. Bouma, B. Pomahac and J. M. Karp, *Nat. Commun.*, 2013, **4**, 1702.

17 H. Jeon, S. Koo, W. M. Reese, P. Loskill, C. P. Grigoropoulos and K. E. Healy, *Nat. Mater.*, 2015, **14**, 918–923.

18 E. Fadaly, I. Massiot, M. Sadeghi, A. Dmitriev and H. Zhao, *Proc. International Conference on Nanotechnology*, 2015.

19 D. S. Wiersma, *Nat. Photonics*, 2013, **7**, 188–196.

20 K. Vynck, M. Burresi, F. Riboli and D. S. Wiersma, *Nat. Mater.*, 2012, **11**, 1017–1022.

21 R. Peretti, G. Gomard, L. Lalouat, C. Seassal and E. Drouard, *Phys. Rev. A*, 2013, **88**, 053835.

22 V. E. Ferry, M. A. Verschuuren, C. V. Lare, R. E. I. Schropp, H. A. Atwater and A. Polman, *Nano Lett.*, 2011, **11**, 4239–4245.

23 E. R. Martins, J. Li, Y. Liu, V. Depauw, Z. Chen, J. Zhou and T. F. Krauss, *Nat. Commun.*, 2013, **4**, 2665.

24 A. Bozzola, M. Liscidini and L. C. Andreani, *Prog. Photovoltaics Res. Appl.*, 2013, **22**, 1237–1244.

25 D. H. Long, I.-K. Hwang and S.-W. Ryu, *Jpn. J. Appl. Phys.*, 2008, **47**, 4527.

26 H. Noh, J. K. Yang, S. F. Liew, M. J. Rooks, G. S. Solomon and H. Cao, *Phys. Rev. Lett.*, 2011, **106**, 183901.

27 D. Van Gestel, I. Gordon and J. Poortmans, *Sol. Energy Mater. Sol. Cells*, 2013, **119**, 261–270.

28 P. Hanarp, D. S. Sutherland, J. Gold and B. Kasemo, *Colloids Surfaces A*, 2003, **214**, 23–36.

29 C. Trompoukis, I. Massiot, V. Depauw, O. El Daif, K. Lee, A. Dmitriev, I. Gordon, R. Mertens and J. Poortmans, *Opt. Express*, 2016, **24**, A191–A201.

30 J. Muller, A. Herman, A. Mayer and O. Deparis, *Opt. Express*, 2015, **23**, A657.

31 C. Becker, D. Amkreutz, T. Sontheimer, V. Preidel, D. Lockau, J. Haschke, L. Jogschies, C. Klimm, J. J. Merkel, P. Plocica, S. Steffens and B. Rech, *Sol. Energy Mater. Sol. Cells*, 2013, **119**, 112–123.

32 T. Saga, *NPG Asia Mater.*, 2010, **2**, 96–102.

33 I. Abdo, C. Trompoukis, J. Deckers, V. Depauw, L. Tous, D. V. Gestel, R. Guindi, I. Gordon and O. E. Daif, *IEEE J. Photovoltaics*, 2014, **4**, 1261–1267.

34 I. Gordon, L. Carnel, D. Van Gestel, G. Beaucarne and J. Poortmans, *Prog. Photovoltaics Res. Appl.*, 2007, **15**, 575–586.

35 P. Campbell and M. A. Green, *J. Appl. Phys.*, 1987, **62**, 243–

249.

36  C. Trompoukis, I. Abdo, R. Cariou, I. Cosme, W. Chen, O. Deparis, A. Dmitriev, E. Drouard, M. Foldyna, E. G-Caurel, I. Gordon, B. Heidari, A. Herman, L. Lalouat, K.-D. Lee, J. Liu, K. Lodewijks, F. Mandorlo, I. Massiot, A. Mayer, V. Miljkovic, J. Muller, R. Orobtchouk, G. Poulain, P. Prod'homme, P. Roca i Cabarrocas, C. Seassal, J. Poortmans, R. Mertens, O. El Daif and V. Depauw, *Phys. Status Solidi A*, 2015, **212**, 140–155.

37  F. Toor, H. M. Branz, M. R. Page, K. M. Jones and H. C. Yuan, *Appl. Phys. Lett.*, 2011, **99**, 103501.

38  A. Rahman, A. Ashraf, H. Xin, X. Tong, P. Sutter, M. D. Eisaman and C. T. Black, *Nat. Commun.*, 2015, **6**, 5963.

39  J. Liu, M. Ashmkhan, G. Dong, B. Wang and F. Yi, *Sol. Energy Mater. Sol. Cells*, 2013, **108**, 93–97.

40  A. Ingenito, O. Isabella and M. Zeman, *Prog. Photovoltaics Res. Appl.*, 2015, **23**, 1649–1659.